Effective water/water contact angle at the base of an impinging jet

Théophile Gaichies,[1] Anniina Salonen,[1] Arnaud Antkowiak,[2] and Emmanuelle Rio[1]
[1]*Laboratoire de Physique des Solides, Universite Paris-Saclay, CNRS, F-91405 Orsay, France*
[2]*Institut Jean le Rond ∂'Alembert, Sorbonne Université, CNRS, F-75005 Paris, France*

(Received 15 November 2023; accepted 16 February 2024; published 27 March 2024)

The base of a jet impinging on an ultrapure water bath is studied experimentally. At the impact point, a train of capillary waves develops along the jet. By performing particle tracking velocity measurements, we show that there is a boundary layer separation between the jet and the meniscus. We thus describe the shape of this meniscus with a hydrostatic model. A striking observation is the existence of an effective nonzero water/water contact angle between the jet and the meniscus. The rationalization of this finite contact angle requires a full description of the shape of the interface. By doing an analytical matching between the meniscus and the jet, we show that the capillary waves can be considered as reflected waves present to ensure pressure continuity. It is finally shown that the value of the apparent contact angle is fixed by energy minimization, with an excellent agreement between prediction and experiment for small jets.

DOI: 10.1103/PhysRevFluids.9.034003

I. INTRODUCTION

Liquid-air interfaces are geometrical objects with an intimate link between their shape and their properties. They give rise to purely geometrical questions such as surface minimization problems [1,2]. A physical illustration is foams, whose mechanical stability is linked to the local bubble packing [3] and whose coarsening is fixed by topology [4,5]. Interfacial geometry can also play a critical role in dynamical situations. For example, the shape of the cusp at the rear of a sliding drop or an entrained film fixes the wetting transition [6,7]. More complex interfacial topologies exist in multiphase flows, such as breaking waves [8] or aeration through weirs or cascades [9]. A paradigm for these flows is the plunging jet, which can entrain air when it impacts a bath [8]. Its geometrical features, such as the shape of the cusp in the viscous case [10,11], or surface disturbances when inviscid [12], control the whole behavior of the system.

In this paper, we focus on the base of water jets impacting a quiescent water bath. We report on an intriguing observation: the apparition of an apparent nonzero contact angle at the water/water junction [see Fig. 1(c)]. We rationalize the presence of this contact angle and provide a description of the whole shape of this interface.

When a water jet plunges in a water bath, a train of stationary capillary waves will be created at its base, and decay upstream [Figs. 1(a) and 1(b)] [14]. Their wavelength can be obtained by equating the phase velocity of the waves with the speed of the jet [15]. The damping coefficient has been modeled and linked to the properties of the fluid [13,16]. However, less attention has been given to the meniscus at the connection between the jet and the bath, where it is clear that there exists an apparent contact angle. This is surprising as the only phases at play are water and air, hence no contact angle is expected.

II. SHAPE OF THE INTERFACE

To study this contact angle, we produce jets of ultrapure water (resistivity larger than 18.2 MΩ cm) with radii R ranging from 50 to 400 μm, using a syringe pump (Harvard Apparatus

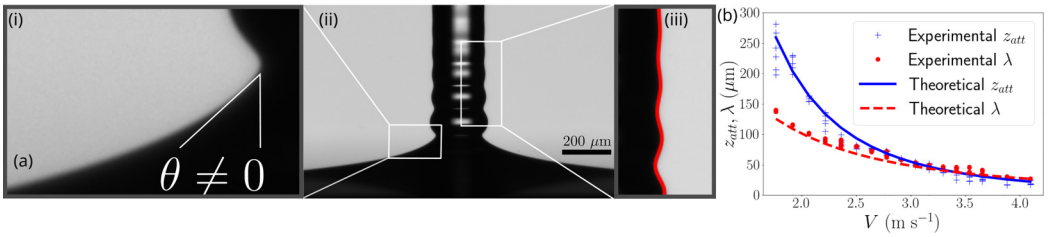

FIG. 1. (a) (ii) Experimental image of a water jet of radius $R = 100$ μm and speed $V = 2.1$ m s^{-1} impacting a bath of water. (iii) Zoom on the capillary waves developing at the jet surface fitted by a function of the form $r(z) = R + a\cos(kz + \varphi)\exp(-\frac{z}{z_{\text{att}}})$. (i) Zoom on the connection between the meniscus and the jet, where the nonzero contact angle appears. (d) Comparison between the values of z_{att} and λ extracted from the experimental fit and the ones calculated with Eq. (6) in Ref. [13] for a jet of radius $R = 160$ μm.

PHD ULTRA) connected to a nozzle when $R < 100$ μm and a pressurized reservoir otherwise. As shown in Ref. [17], a small amount of surfactants in the recipient bath modifies significantly the wave pattern, so great care was taken to avoid contamination of the ultrapure water in our experiments. The pressure in the reservoir is imposed by a pressure controller (Elveflow OB1 Mk4) connected to a network of compressed air. These setups can create laminar jets with speeds between 1.9 and 8 m s^{-1} for $R < 100$ μm and between 1.4 and 5 m s^{-1} for bigger ones. The base of the jet is imaged using telecentric lenses (SilverTl 2× or 4× Edmund Optics) to obtain sharp interfaces and a digital camera (Basler a2A1920-160umPRO). The images were typically taken with an exposure time of 700 μs.

Measuring the observed contact angle is not straightforward, as it is not possible to place the contact line between the jet and the meniscus in a nonarbitrary manner. To overcome this problem, we propose to measure the contact angle by fitting the shape of the interface. Despite the jet having a speed of a few meters per second, the meniscus at the base of the jet looks very similar to the one climbing a static fiber plunged in a liquid bath [visual comparison in Figs. 2(a) and 2(b)], as was previously noticed by Patrascu *et al.* [13]. We performed particle tracking velocimetry (PTV) measurements below the interface, using small silica particles (of radius between 30 and 80 μm), and a fast camera (Photron FASTCAM NOVA S9) recording 6000 images per second. These images

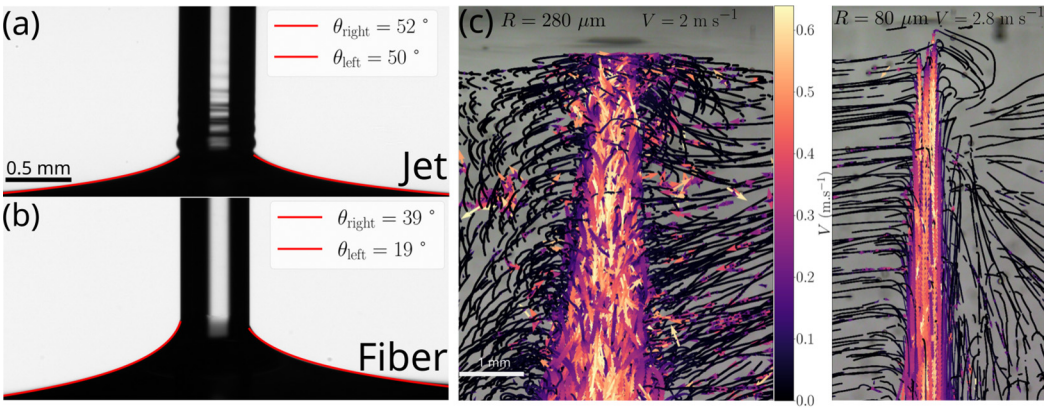

FIG. 2. (a) Fit of the meniscus, on the right and on the left, by Eq. (1) for a jet of radius $R = 280$ μm and speed $V = 2.65$ m s^{-1} and for (b) a glass fiber of $R = 250$ μm. (c) Results of the PTV experiments under the water surface for a jet of radius $R = 280$ μm and speed $V = 2$ m s^{-1} and a jet of radius $R = 80$ μm and speed $V = 2.8$ m s^{-1}.

were then analyzed with PYTHON. The results can be seen in Figs. 2(c) and 2(d) for two different jet radii and velocities. The measurements confirm that there is a boundary layer separation between the dynamic jet and the static meniscus, with a typical velocity ratio of 20 between the velocity in the dynamic jet and in the still zone of the meniscus. This is consistent with the observation and description of Sebilleau *et al.* [18], where this boundary layer separation is expected for $\mathrm{Re} > 60$ and has been observed for jets with radii 2 mm $< R <$ 5 mm and $\mathrm{We} = \frac{\rho V^2 R}{\gamma} < 0.14$. We show that their findings hold for smaller jets, and for higher Weber numbers (up to 15 in our experiments). This justifies the use of hydrostatic equations to describe the shape of the meniscus.

The shape of the static meniscus is fixed by a balance between the hydrostatic pressure $\rho g z$, with ρ the liquid density, g the acceleration of gravity, z the surface elevation, and the Laplace pressure $\gamma \mathcal{C}$, with γ the liquid/air surface tension and $\mathcal{C}$ the curvature of the interface. The typical length scale of the meniscus is thus the capillary length $\ell_c = \sqrt{\frac{\gamma}{\rho g}}$. An equation for $z(r)$, with r the coordinate in the radial direction, in the nonlinear part of the meniscus attached to a fiber of radius r_0 with a nonzero contact angle has been proposed by James [19]. The linear small slope solution is $z(r) = A K_0(\frac{r}{l_c})$, where A is a constant and K_0 a modified Bessel function of the second kind of order zero. By matching it with the equation of a catenoid satisfying the boundary condition $z'(r_0/r_0) = -\mathrm{cotan}(\theta)$ where θ is the contact angle, he obtains, in the vicinity of the fiber,

$$z(r) = r_0 \cos(\theta)\left(- \ln(\epsilon) + \ln(4) - \Gamma - \ln\left\{ \frac{r}{r_0} + \left[\left(\frac{r}{r_0} \right)^2 - \cos^2(\theta) \right]^{\frac{1}{2}} \right\} \right), \tag{1}$$

where $\epsilon = \sqrt{\frac{\rho g R^2}{\gamma}}$ is the square root of the Bond number and Γ is Euler's constant. We use James' equation to fit the meniscii in Figs. 2(a) and 2(b). The contact angle is used as a free parameter and can be different on the right and on the left. This leads to slightly different values of the contact angle on the jet, which will be taken into account while evaluating the error bars. On the fiber, the difference is larger, probably due to impurities at its surface. The agreement between the fit and the experimental shape confirms that this region can be considered as static, and that there exists a nonzero contact angle between the meniscus and the jet. Replacing directly the fiber radius r_0 in James' equation with the jet radius R proves unsatisfactory, because the actual radius is altered with the capillary wave field. We thus need to write proper matching conditions between the capillary wave field and the static meniscus.

In the following, we propose a matching between James' description of the meniscus and the jet decorated with capillary waves. The parameters needed to describe the meniscus using James' equation are r_0 and θ. The capillary wave field is approximated by an attenuated sinusoidal wave $r(z) = R + a\cos(kz + \varphi)\exp(-\frac{z}{z_{\mathrm{att}}})$, with $k = \frac{2\pi}{\lambda}$ the wave number, λ the wavelength, a the amplitude, φ a phase shift, and z_{att} the attenuation length. k and z_{att} are predicted by the model of Patrascu (Eq. (6) in Ref. [13]). It agrees very well with the fitted values of z_{att} and λ, as can be seen in Fig. 1(d). We then have five unknowns θ, r_0, z_0, φ, and a. The first matching condition is the radial matching position, which gives $r_0 = r(z_0)$. The height matching position z_0 is given by James' equation $z_0 = z(r_0)$. The slope matching yields $\frac{\partial r}{\partial z} = -\tan(\theta)$. The last condition is the matching between the jet curvature

$$\kappa_{\mathrm{jet}} = \frac{1 + r'(z)^2 - r(z) r''(z)}{r(z)[1 + r'(z)^2]^{3/2}}$$

and the meniscus curvature $\kappa_{\mathrm{m}} = 0$, as the meniscus is a catenoid. Practically, we used a linearized version of κ_{jet} as full nonlinear computations did not show significant differences.

This curvature matching is in fact a pressure matching between the jet, which has an overpressure $\Delta P = \frac{\gamma}{R}$, and the meniscus, which has an underpressure $\Delta P = -\rho g z$. Capillary wave emission stems from this pressure mismatch. The reflected waves lower the curvature of the impinged jet base to accommodate with the meniscus' pressure, as sketched in Fig. 3(a). This is similar to the stationary wave rippling the air cavity entrained behind an object dropped in a liquid [20]. In this

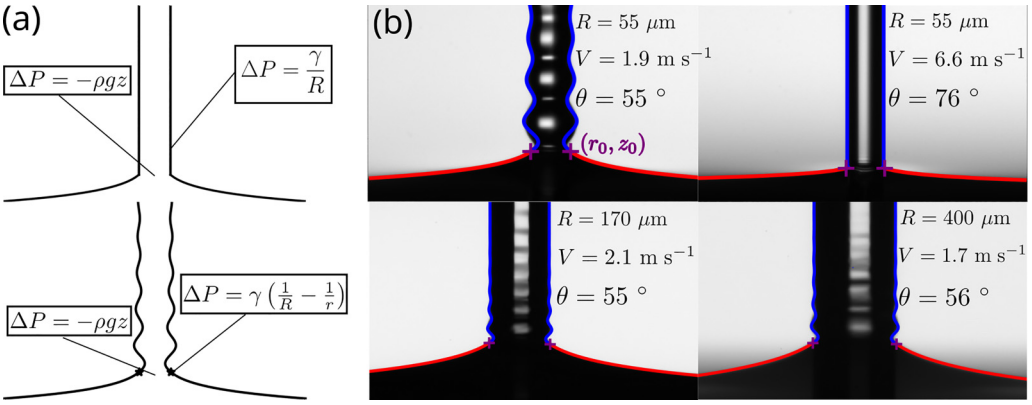

FIG. 3. (a) Sketch of the jet impacting a bath. In the first virtual case, a straight jet connects to the meniscus, and exposes the impossibility of a pressure continuity between the two regions. In the second case, the capillary waves allow for pressure continuity. (b) Fitted interfaces of jets of various radii and speeds. The red line is the fitted meniscus, the blue line the wave field with the calculated amplitude, and the violet cross the calculated matching point (r_0, z_0).

case, a reflected stationary wave is needed so that the cavity is attached to the side of the moving object. These situations are reminiscent of classical problems in wave physics, where boundary conditions are impossible to meet without a reflected wave [21].

With five unknowns but only four matching conditions, the problem is underconstrained as stated. However, if we set a θ, we can get all the other values owing to the following system,

$$\begin{aligned} r_0 &= \frac{R\left[R^2 + z_{\text{att}}^2(k^2R^2 - 2) + 2z_{\text{att}}R\tan(\theta)\right]}{R^2 + z_{\text{att}}^2(k^2R^2 - 1)}, \\ z_0 &= r_0\cos(\theta)\left[\log\left(\frac{4R}{r_0\epsilon[1 + \sin(\theta)]}\right) - \Gamma\right], \\ \varphi &= -kz_0 + \arctan\left(\frac{r_0 - R - z_{\text{att}}\tan(\theta)}{kz_{\text{att}}(R - r_0)}\right), \\ a &= \frac{(r_0 - R)\exp(z_0/z_{\text{att}})}{\cos(kz_0 + \varphi)}, \end{aligned} \tag{2}$$

where φ can be shifted by π to get a positive amplitude. To test that our equations of matching indeed set the amplitude of the capillary waves, we follow this fitting procedure: For a jet of given R and V, we first get k and z_{att} by fitting the wave pattern at the base of the jet, or from the Patrascu equation (that only depends on R and V) when the waves become barely visible on our images. This fixes $r_0(\theta)$ through Eq. (2). We then obtain θ by fitting the meniscus with James' equation.

When θ is fitted, we inject it in system (2) and deduce the values of z_0, φ, and a. In Fig. 3(b), the resulting wave field is plotted on the image, together with James' equation for the fitted θ. We can see that, for various radii and jet velocities, the obtained amplitude agrees very well with the experimental one. This confirms that the pressure matching between the meniscus and the jet sets the amplitude of the capillary wave field.

III. PREDICTION FOR THE CONTACT ANGLE

To get a complete model of the interface, we miss a prediction for θ, as all θ are compatible with our equations of matching. However, the total energy of the system depends on θ. As can be seen in Fig. 4(a), when θ is small, the meniscus joins the jet at a higher altitude, resulting in an

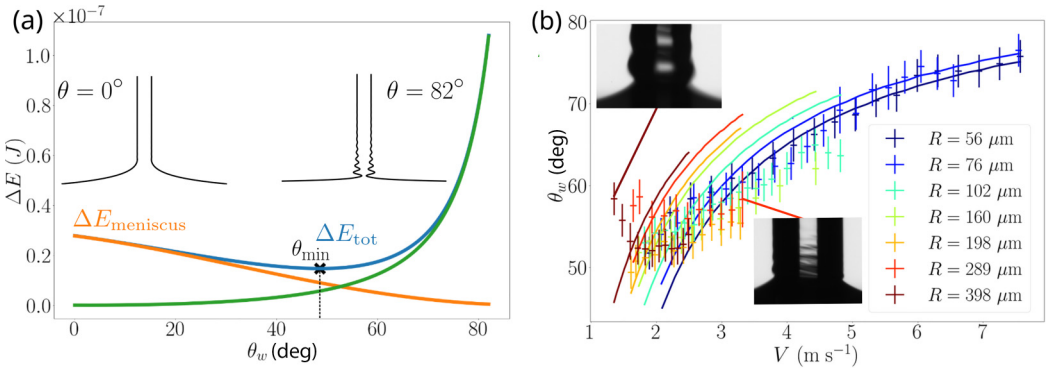

FIG. 4. (a) Energy excess of the meniscus (ΔE_{jet}), of the jet ($\Delta E_{\text{meniscus}}$), and their sum ($\Delta E_{\text{tot}}$) plotted against the speed for a jet of radius $R = 190$ μm. The inserted sketches show the difference between the shape of the interface for a low and high contact angle. (b) Apparent contact angle fitted and predicted by our model for jets of various radii, plotted against the speed of the jet. The two experimental images show two reasons for the deviation from our model, the first one being instationarity (at the top) and the second one (at the bottom) the loss of axisymmetry, even when the stationarity is restored.

excess surface compared to a flat meniscus. When θ is large, the amplitude of the capillary waves is larger, so the excess of surface compared to an unperturbed jet is higher. The kinetic energy excess caused by the capillary waves is equal to the surface energy excess according to Chandrasekhar [see Eqs. (154) and (57) of Chap. XII in Ref. [22]]. It is then possible to calculate the difference in energy ΔE with a virtual cylindrical waveless jet and flat meniscus as a function of θ,

$$\Delta E_{\text{tot}}(\theta) = 2\pi\gamma\left\{2\int_{z_0(\theta)}^{\infty}\left[R(z,\theta)\sqrt{1+\frac{\partial R(z,\theta)}{\partial z}^2}-R\right]dz+\int_{r_0(\theta)}^{\infty} r\left(\sqrt{1+\frac{\partial z(r,\theta)}{\partial r}^2}-1\right)dr\right\}$$
$$+\rho g\int_{r_0(\theta)}^{\infty}\pi r z(r,\theta)^2 dr, \tag{3}$$

where the last term accounts for the gravitational potential energy of the meniscus [23]. The sum of the jet energy, ΔE_{jet} [first term in Eq. (3)] and the meniscus energy $\Delta E_{\text{meniscus}}$ (second and third term in Eq. (3)) is plotted in Fig. 4(a), revealing a value θ_{min} which minimizes ΔE_{tot}. This θ_{min} depends on V and R as these variables set k and z_{att}, which affect ΔE_{jet}. In Fig. 4(b), the prediction of θ_{min} is plotted together with the experimental data as a function of V for different radii. The uncertainty for the experimental value of θ_{w} comes from the numerical uncertainty on the fit of the meniscus. For small jets ($R = 56$ μm and $R = 76$ μm), the model agrees well with the experiments without any fitting parameters, especially when $V > 3$ m s^{-1}. For lower speeds, a/R is not negligible and capillary waves are not well described by an attenuated sinusoid [24] [see the first image in Fig. 3(b)], so we expect a bigger difference with our model. For wider jets, non-stationarities, and a certain degree of swirl [13] can appear [see Fig. 4(b)], which result in deviations from our model, as our assumptions of stationarity and axisymmetry are no longer fulfilled.

IV. CONCLUSION

In conclusion, the observation of an apparent contact angle when a jet impacts a bath has been rationalized. Capillary waves are due to a pressure matching between the jet and the meniscus, and energy minimization fixes the effective contact angle at least. Our data are in excellent agreement with this prediction for tiny jets. Discrepancies appearing for wider jets underline the necessity to better understand the nonstationary and asymmetric regimes.

ACKNOWLEDGMENTS

We are grateful to Christophe Raufaste for stimulating discussions and Alice Etienne Simonetti for careful code reviewing.

[1] R. Courant, The existence of a minimal surface of least area bounded by prescribed Jordan arcs and prescribed surfaces, Proc. Natl. Acad. Sci. USA **24**, 97 (1938).
[2] J. A. F. Plateau, *Statique Expérimentale Et Théorique Des Liquides Soumis Aux Seules Forces Moléculaires* (Gauthier-Villars, Paris, 1873), Vol. 2.
[3] S. Heitkam, W. Drenckhan, and J. Fröhlich, Packing spheres tightly: Influence of mechanical stability on close-packed sphere structures, Phys. Rev. Lett. **108**, 148302 (2012).
[4] J. von Neumann, in *Metal Interfaces*, edited by C. Herring (American Society for Metals, Cleveland, 1952), pp. 108–110.
[5] S. Hilgenfeldt, A. M. Kraynik, S. A. Koehler, and H. A. Stone, An accurate von Neumann's law for three-dimensional foams, Phys. Rev. Lett. **86**, 2685 (2001).
[6] N. Le Grand, A. Daerr, and L. Limat, Shape and motion of drops sliding down an inclined plane, J. Fluid Mech. **541**, 293 (2005).
[7] J. H. Snoeijer, G. Delon, M. Fermigier, and B. Andreotti, Avoided critical behavior in dynamically forced wetting, Phys. Rev. Lett. **96**, 174504 (2006).
[8] K. T. Kiger and J. H. Duncan, Air-entrainment mechanisms in plunging jets and breaking waves, Annu. Rev. Fluid Mech. **44**, 563 (2012).
[9] D. A. Ervine, Air entrainment in hydraulic structures: A review, Proc. Inst. Civ. Eng.: Water Maritime Energy **130**, 142 (1998).
[10] J. Eggers, Air entrainment through free-surface cusps, Phys. Rev. Lett. **86**, 4290 (2001).
[11] É. Lorenceau, D. Quéré, and J. Eggers, Air entrainment by a viscous jet plunging into a bath, Phys. Rev. Lett. **93**, 254501 (2004).
[12] Y. Zhu, H. N. Oğuz, and A. Prosperetti, On the mechanism of air entrainment by liquid jets at a free surface, J. Fluid Mech. **404**, 151 (2000).
[13] C. Patrascu and C. Balan, Decay of stationary capillary waves on impinging liquid jets, Phys. Fluids **33**, 022109 (2021).
[14] D. Sklavenites, Wave patterns on a water column, Am. J. Phys. **65**, 225 (1997).
[15] J. Lighthill, *Waves in Fluids* (Cambridge University Press, Cambridge, UK, 1978).
[16] K. M. Awati and T. Howes, Stationary waves on cylindrical fluid jets, Am. J. Phys. **64**, 808 (1996).
[17] M. J. Hancock and J. W. M. Bush, Fluid pipes, J. Fluid Mech. **466**, 285 (2002).
[18] J. Sébilleau, L. Limat, and J. Eggers, Flow separation from a stationary meniscus, J. Fluid Mech. **633**, 137 (2009).
[19] D. F. James, The meniscus on the outside of a small circular cylinder, J. Fluid Mech. **63**, 657 (1974).
[20] T. Grumstrup, J. B. Keller, and A. Belmonte, Cavity ripples observed during the impact of solid objects into liquids, Phys. Rev. Lett. **99**, 114502 (2007).
[21] J. Billingham and A. C. King, *Wave Motion*, Cambridge Texts in Applied Mathematics No. 24 (Cambridge University Press, Cambridge, UK, 2000).
[22] S. Chandrasekhar, *Hydrodynamic and Hydromagnetic Stability* (Courier Corporation, North Chelmsford, MA, 2013).
[23] The meniscus energy term has here been computed using the uniformly valid composite solution of James (see Sec. 6 of Ref. [19]).
[24] J.-M. Vanden-Broeck, T. Miloh, and B. Spivack, Axisymmetric capillary waves, Wave Motion **27**, 245 (1998).